EFFECTS OF TEMPERATURE ON AQUEOUS FREEFORM EXTRUSION FABRICATION

Jie Li[1], Ming C. Leu[1] and Gregory E. Hilmas[2]
[1]Department of Mechanical and Aerospace Engineering
[2]Department of Ceramic Engineering
Missouri University of Science and Technology, Rolla, MO 65409
REVIEWED

Abstract

An experimental study was conducted to investigate the effect of temperature on ceramic parts produced by paste extrusion based additive manufacturing followed by sintering. A computer-controlled gantry system equipped with a piston extruder was used to extrude aqueous alumina paste. The system includes a temperature control subsystem that allows for freeform extrusion fabrication inside a low-temperature (<0°C) chamber. It can also be used for fabricating parts on a hot plate at ambient or higher temperatures (≥20°C). Test specimens were fabricated from aqueous aluminum pastes at -20°C in the low-temperature chamber and also on the hot plate at 40°C. The minimum angles achievable by these two processes for part fabrication, without use of support material, were compared. Also compared were the relative density and mechanical properties of the parts obtained after sintering. Microstructures were examined via scanning electron microscopy in order to obtain a deeper understanding of the effect of fabrication temperature.

Introduction

Since the mid-1980s, Solid Freeform Fabrication (SFF) technology has been developed with the potential of becoming an efficient and inexpensive manufacturing technique to produce polymer, metal and ceramic parts in small volumes [1, 2]. SFF techniques for ceramic component fabrication include Ink-jet Printing [3], Stereolighography (SLA) [4], 3D Printing (3DP) [5, 6], Selective Laser Sintering (SLS) [7], Robocasting [8] and Fused Deposition of Ceramics (FDC) [9, 10]; see Table 1. Most of SFF techniques for ceramic component fabrication involve the use of high concentration (>40%) of organic binders that needs to be removed during post processing, which generate harmful wastes for the environment. One of extrusion deposition techniques of ceramic is FDC, which is capable of fabricating dense ceramic parts with good surface accuracy but uses a relatively large amount (40-50%) of organic chemicals as binders [10].

Use of an aqueous process with a much lower binder amount would be more environmentally friendly. Robocasting is one well-known technology, initially developed at Sandia National Laboratories, for fabrication of ceramics and ceramic composites. This process could extrude 50~65% high solids loading aqueous slurry with less than 1% organic binder. For fabricating solid, dense parts, Robocasting uses a heating source (a 40^{o}C hot plate) to dry the paste during extrusion to form a 3D part [8]. The relative density and flexural strength reported were 93.7% and 310 MPa for Al_2O_3 samples [8, 11].

Another aqueous SFF technology is Freeze-form Extrusion Fabrication (FEF), which was developed by researchers at Missouri University of Science and Technology. In the FEF process, a high solids loading (>50%) aqueous paste containing 1~4 vol% organic additives is deposited inside a freezing chamber (<0^{o}C) to solidify the paste after it is extruded. Freeze drying is then

used to prevent crack formation during the process of removing water content. The flexural strength reported was 219 MPa for Al_2O_3 samples [12, 13].

Table 1 Popular SFF techniques for ceramic material

Process	Method	Materials	References
Selective Laser Sintering (SLS)	Sinter ceramic-binder mixed in powder bed	Al_2O_3, SiC, $ZrSiO_4$	[7]
3D printing (3DP)	Print binder solution on ceramic powder bed	Al_2O_3, Si_3N_4	[5, 6]
Stereolighography (SLA)	Cure mixed resins with ceramic particles	SiO_2, PZT, Al_2O_3	[4]
Ink-jet Printing	Print colloidal droplets	Al_2O_3, Si_3N_4, ZrO_2	[3]
Fused Deposition Ceramic (FDC)	Print melt ceramic particle-filled polymer	Al_2O_3, Si_3N_4,	[9, 10]
Robocasting (In air/oil)	Print organic/non-organic concentrated colloidal gel	Al_2O_3, PZT, SiO_2	[8, 11]

This research systematically studied the effect of temperature on the mechanical properties of freeform extrusion fabricated ceramics from aqueous pastes. A custom-built 3D gantry system was equipped with a cooling sub-system and could include a hot plate for part fabrication. This system was used to print aqueous alumina paste by freeform extrusion fabrication on a 40°C plate inside a room-temperature chamber and on a -20°C plate inside a -20°C temperature chamber, in order to study the effect of temperature on fabrication results. In this paper, the first condition (fabricating on a 40°C plate in a room-temperature environment) would be referred to 'at 40°C', and the second condition (fabricating on a -20°C plate inside a -20°C temperature chamber) would be referred to 'at -20°C'. A 60% solids loading aqueous Al_2O_3 paste was used as the part material in all of the experiments. The relative density, mechanical properties, part accuracy, and minimum deposition angle of Al_2O_3 parts fabricated at different temperatures were investigated. SEM and optical images were used to help understand the temperature effect on the microstructure of the fabricated parts.

Experimental Setup and Methods

Machine Overview

The experimental system consists of a motion subsystem, a control subsystem, and extrusion devices. A picture of the overall system is shown in Fig. 1a. The system has three linear axes (Parker Hannifin, Daedal 404 XR) driven by three stepper motors (Empire Magnetics). In this research, a single extruder is used to extrude aqueous alumina paste. The paste is extruded onto a substrate that moves in the x and y axes. After deposition, the paste would solidify in a freezing environment as shown in Fig. 1b or dry on a hot plate set at 40°C as shown in Fig. 1c.

When the fabrication of one layer is completed, the gantry moves up by one layer thickness. These processing steps are repeated until the entire part is formed.

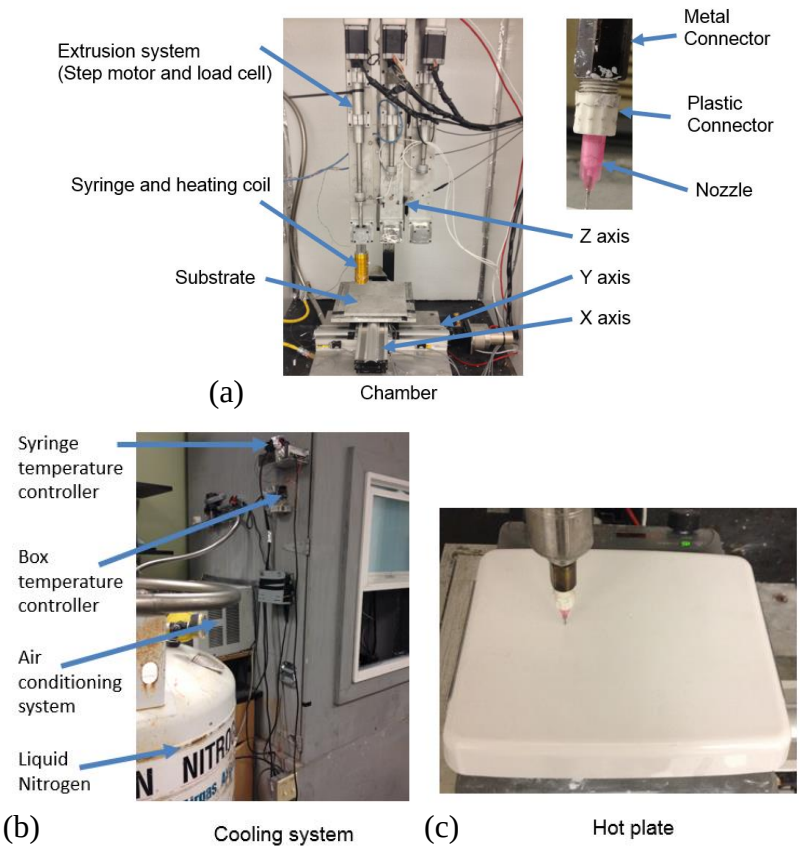

Figure 1. Experimental setup of the machine: (a) overview of machine, (b) the cooling system and (c) the hot plate

Material Characterization

The 60% solids loading alumina paste was used in all of the experiments in this study. The particle size were analyzed using a Microtrac Particle Size Analyzer (S3500, Microtrac), and the particle surface area was measured using a NOVA 2000e instrument (Quantachrome Instruments). The paste consisted of a combination of Al_2O_3 powder (A-16SG, ALMATIS, 0.34 µm, 9.44 m^2/g), glycerol (Aldrich), DARVAN® C-N (ammonium polymethacrylate, Vanderbilt Minerals), Methocel*F4M (methylcellulose, Dow Chemical) and deionized water. The slurry was mixed with Darvan C and glycerol and subsequently ball-milled for 10 hours to break up agglomerates and produce a uniform mixture. Darvan C with a negative surface charge was used as a dispersant to mitigate the Van Der Waals forces between particles [14-16]. Glycerol (20 wt%) was used to prevent the growth of large ice crystals and freezing defects associated with water solidification [17]. Methocel was dissolved in water at 70°C after 5 minutes of mechanical stirring to form a 60 vol% solids loading paste and was chosen as a binder to increase the paste viscosity and assist in the formation of a stronger green body after drying. A vacuum mixer (Whip Mix, Model F) was used to remove air bubbles by degassing for 10 minutes.

Post-processing

The water content in the test bars fabricated at -20°C was removed via sublimation using a freeze dryer (Virits, Model Genesis 25XL). When building the part on a hot plate, the water inside the paste evaporated at 40°C to increase solids loading, which provides the strength for layer-by-layer fabrication to form 3D parts.

The results of thermogravimetric analysis (TGA) and sintering tests were used to determine the debinding and sintering schedule. After drying, the samples were pyrolyzed to remove the remaining organics using a 0.5°C/minute ramp up to 500°C with a hold of 2 hours. Next, the samples were sintered to 1,550°C using a heating rate of 10°C/minute, held for 2 hours, and then cooled to room temperature.

Mechanical Properties and Microstructure

The fabricated samples, after sintering, were ground by diamond grinding according to ASTM C-1161 standard "A" bars (2x1.5x20 mm^3). Four-point bending tests were performed on a screw-driven mechanical frame (Instron, Model 5881) to measure the flexural strength and elastic modulus. A micro-hardness tester (Struers, Model Duramin-5) was used to measure hardness. The hardness was measured using a load of 1 kg, and five measurements were collected for each specimen on a 0.25 μm diamond polished surface.

Bars fabricated at 40°C, -20°C, and -20°C without using a nozzle for extrusion. Three bars were printed to test the green body density. After drying and binder removal, Archimedes method (in water) was used to measure the green body density and relative density after sintering.

The microstructures of fabricated bars were studied and compared in order to understand the effect of printing flaws and formation of ice crystal voids. Samples were polished to a 0.25 μm surface finish, and SEM was used to examine the microstructure of each sample.

Results and Discussion

Overall Effects of Temperature

When the paste printing was done on a plate (without heating) at room temperature without using a hot plate, the drying rate was not fast enough. In this case, a large 3D part being fabricated will deform or even collapse. In contrast, the drying rate of the extruded material on a 60°C plate (in a room temperature environment) was significantly higher than printing on a 40°C plate. Moisture distributed unevenly in the part's body as a result of the temperature variations and non-uniform drying led to part warping or cracking. Thus, 40°C was used for the hot plate temperature.

Ten bars (6x7x60mm^3) were fabricated at 40°C and ground to the standard B bar size. The average flexural strength of bars fabricated at 40°C was 253 MPa and the average elastic modulus was 327 GPa as listed in Table 2. These bars have lower flexural strength than pressed bars (370~390 MPa). A few printing flaws and air bubbles in the paste caused ~6% porosity, which markedly reduced mechanical strength after sintering. Ten additional single walls having only one filament at each layer were fabricated in an attempt to eliminate printing flaws. The difference between the nozzle printed bar's relative density and the flaw-free single wall's relative density was smaller than 1% (see Table 2). Thus, the air bubble in the paste was the main reason for the approximately 3% porosity of parts fabricated at 40°C.

A heating coil (see Fig. 1a) was used to maintain the paste warm when printing was done in the freezing chamber. The extruded ceramic paste could freeze at -20°C and the required waiting time for one filament (0.5*0.74*60 mm^3) was approximately 10 seconds. One critical issue in

printing under a freezing environment was clogging, which often occurred because the paste froze inside the nozzle before it was extruded.

Six bars (6x7x60 mm^3) were fabricated at -20°C and ground to the standard B bar size. The average flexural strength of bars fabricated at -20°C was 153 MPa, and the average elastic modulus was 327 GPa (see Table 3). Ice crystals, printing flaws, and air bubbles were primarily responsible for this kind of low flexural strength. Bars fabricated at -20°C tended to have more flaws than those fabricated at 40°C. Two factors were responsible for this increased number of flaws. First, clogging led to discontinued printing and voids. Second, the paste extruded at -20°C solidified faster than drying of the paste extruded at 40°C, leaving the time required to fill the voids between filaments too short. Single walls were also printed to measure the part density without printing flaws, and it indicated that ice crystal voids also contributed to the lower density.

Table 2. Mechanical properties and relative density of bars fabricated at 40°C

#	Flexural Strength (MPa)	Flexural Modulus (GPa)	Relative Density (%)	Relative Density of Single Walls (%)
1	327	352	94.40	93.63
2	290	333	96.30	95.01
3	276	341	92.20	94.81
4	268	330	92.62	94.73
5	262	349	94.03	94.47
6	246	320	94.14	94.86
7	244	286	92.24	94.55
8	234	316	94.04	94.34
9	207	306	93.67	94.32
10	177	337	94.15	96.85
Average	253	327	93.78	94.76
Standard Deviation	42	20	1.22	0.83

Table 3. Mechanical properties and relative density of bars fabricated at -20°C

#	Flexural Strength (MPa)	Flexural Modulus (GPa)	Relative Density (%)	Relative Density of Single Walls (%)
1	192	242	88.74	86.52
2	166	217	86.91	87.58
3	161	274	88.83	87.30
4	154	244	88.06	84.67
5	132	246	89.12	86.36
6	116	197	85.74	86.71
Average	153	237	87.90	86.52
Standard Deviation	24	24	1.21	0.93

Two bars were fabricated on a 0°C plate inside a -20°C chamber. The relative density and flexural strength of the bars were 86.5% and 48 MPa, respectively. The bars' mechanical properties were much lower than printing on a -20°C plate because large-sized voids formed from ice crystals as illustrated in Fig. 2a.

Five 'big' bars were printed at -20°C directly from a syringe without using a nozzle to avoid printing flaws. Each of these 'big' bars contained only one filament, and the size was approximately 10x10x60 mm^3 after deposition. After post-processing, the sample was ground to the standard B bar size. The 'big' bars did not contain any printing flaws, but the flexural strength and the elastic modulus of these bars (listed in Table 4) were even lower than the bars printed with a nozzle at -20°C (Table 3). The low strength is thought to be due to the relatively large filament having an uneven temperature gradient inside the filament. The temperature inside the filament and filament's surface temperature were measured using a thermometer. As shown in Fig. 3, the temperature inside the big filament was warmer than the filament's surface temperature**.** Ice crystal formation was observed as shown in Fig. 2b. Apparently larger-sized crystals formed when the temperature is warmer (between 0°C and -20°C).

Table 4. Mechanical property and relative density of bars fabricated at -20°C without using a nozzle

#	Flexural Strength (MPa)	Flexural Modulus (GPa)	Relative Density (%)
1	122	186	86.19
2	104	210	85.23
3	77	179	85.01
4	69	139	86.07
5	60	149	85.46
Average	86	173	85.59
Standard Deviation	23	26	0.46

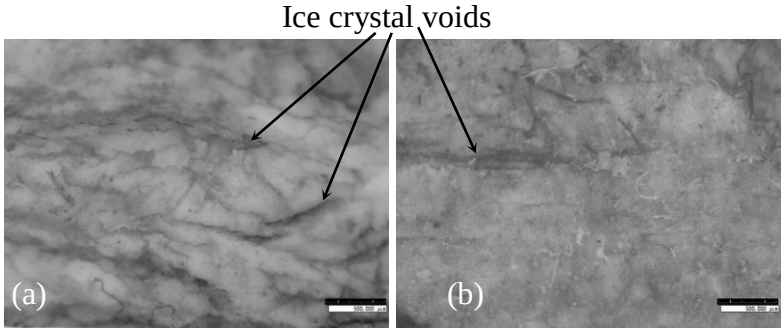

Figure 2. Cross-section view (a) bar fabricated on a 0°C plate and (b) bar fabricated at -20°C without using a nozzle

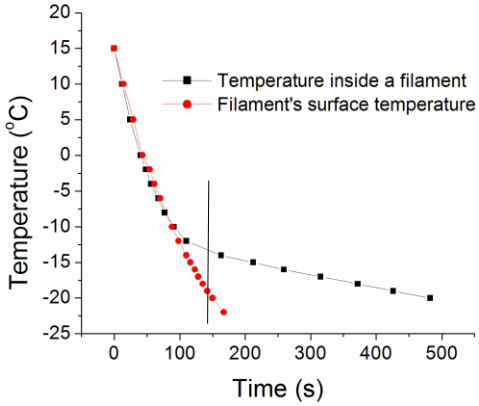

Figure 3. Non-uniform temperature inside the filament fabricated at -20°C without using a nozzle

Figure 4 provides a comparison of flexural strengths and relative densities for bars fabricated under three different conditions: 40°C, -20°C, and -20°C without using a nozzle. The relative density of bars fabricated at 40°C was 94.76%, which was higher than the bars fabricated at -20°C with/without using a nozzle (86.52% / 85.59% in relative density). The relative density of bars fabricated at -20°C with/without using a nozzle had only small difference (1%). However, the flexural strength of bars fabricated at -20°C without using a nozzle was 40% lower than the flexural strength of bars fabricated at -20°C with using a nozzle (see Fig. 4a).

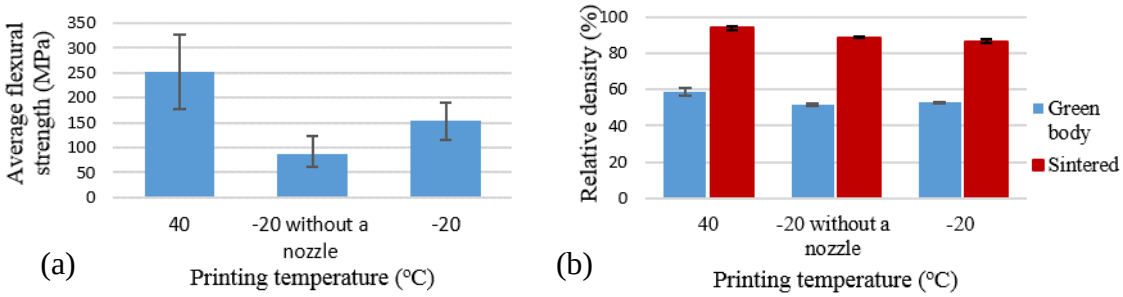

Figure 4. Comparison of (a) mechanical properties and (b) relative density of parts fabricated by three different methods

The hardnesses of samples fabricated at 40°C and -20°C were 16.78±0.43 GPa (1712.04±44.06 Kg/mm^2) and 14.36±0.85 GPa (1465.46±86.26 Kg/mm^2), respectively.

Part Accuracy and Minimum Deposition Angle

Bars were printed at 40°C and -20°C to compare part accuracy as shown in Fig. 5. The dimensions were measured for the green (after drying) and sintered bars, as listed in Table 5. Bars fabricated at -20°C had 1.5% to 3% more expansion than bars fabricated at 40°C because each filament contained approximately 40 vol% water and freezing of water increased the total volume.

The minimum deposition angle here refers to the angle that can be achieved between the substrate and the slope of a hollow cone without collapsing, as illustrated in Fig. 6a. This angle reflects the capability of a freeform extrusion fabrication process to build 3D parts without need of support material [18]. Two sets of tests were conducted to fabricate cones with different bottom diameters to find the minimum deposit angle. In each set of tests, hollow cones were fabricated

using the bottom diameters of 38 mm, 51 mm and 64 mm. The cone angle was varied from 60° to 20° by 5° decrements to measure the angle at which the cone collapsed and then the angle was increased from the failure angle by 2° increments to determine the minimum deposition angle. The part was printed with a 6 mm/s table speed. As shown in Table 6, the parts printed at -20°C had a smaller deposition angle than printed at 40°C. This is because each extruded filament would solidify faster at -20°C, providing support strength to prevent part from collapsing.

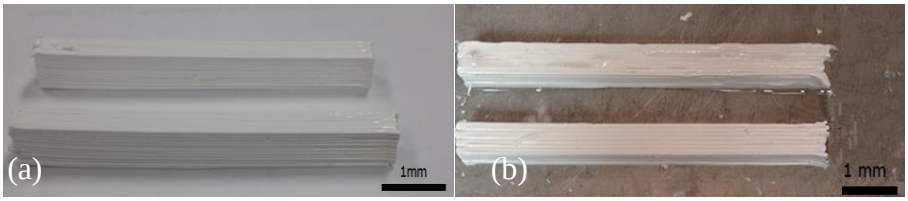

Figure 5. Bars fabricated at (a) 40°C and (b) -20°C

Table 5. Shrinkage in the green body and sintered part

		W (mm)	H (mm)	L (mm)
CAD		5.6	7.8	70
Printed at 40°C	Green bar	6.03 ±0.12	8.03±0.13	71.12±0.12
	Linear shrinkage of green bar	-7.68±2.06%	-2.91±01.64%	-1.60±0.18%
	After sintering	5.05±0.16	7.24±0.03	60.54±0.16
	Linear shrinkage after sintering	9.88±2.90%	7.22±0.44%	13.51±0.23%
Printed at -20°C	Green bar	6.17±0.10	8.19±0.02	72.37±0.20
	Linear shrinkage of green bar	-10.24±1.69%	-5.04±0.26%	-3.39±0.29%
	After sintering	5.04±0.15	7.00±0.11	58.78±0.21
	Linear shrinkage after sintering	10.06±2.70%	10.21±1.39%	16.02±0.29%

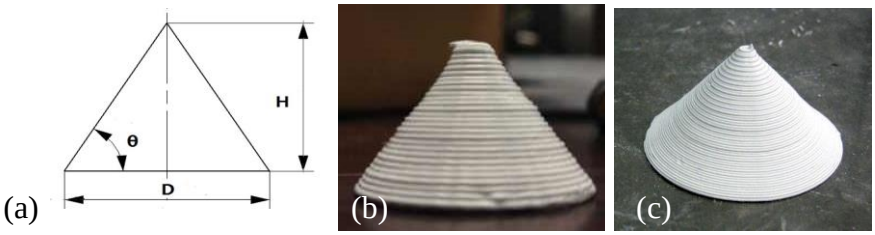

Figure 6. Hollow cone: (a) θ is the minimum deposition angle, D is the bottom diameter and H is the height of cone, (b) fabricated cone at 40°C and (c) fabricated cone at -20°C [18].

Table 6. Minimum deposition test results

	Bottom Diameter = 38 (mm)	Bottom Diameter = 51 (mm)	Bottom Diameter = 64 (mm)
	Minimum deposition angle θ (°)		
Fabrication at 40°C	50	52	55
Fabrication at -20°C [18]	28	26	24

Mechanical Properties

Ten standard A bars were fabricated at both 40°C and -20°C and were subjected to the same post-processing. The bars fabricated at 40°C and -20°C had a green density of 58.49% and 51.35%, respectively. As shown in Tables 7 and 8, bars fabricated at -20°C achieved an average strength of 300 MPa, whereas the average strength of bars fabricated at 40°C was 338 MPa.

The theoretical flaw size was calculated by using equation (1), which is Griffith criterion. Assuming the fracture toughness to be 4 MPa*$m^{1/2}$ [19], and a shape factor that is characteristic of joined particles, Griffith criterion is:

$$\sigma_f = \frac{K_{IC}}{Y\sqrt{c}} \quad (1)$$

where K_{IC} is the fracture toughness, Y= $\pi^{1/2}$ and c is one half of the maximum flaw size. Based on the results of standard A bar test (see Tables 7 and 8), the calculated and measured maximum flaw size for bars fabricated at -20°C and 40°C are given in Table 9. Example flaws for bars fabricated at -20°C and 40°C are illustrated in Fig. 7. As shown in Fig. 7a, the bars fabricated at -20°C have printing flaws (in triangular shape) in the cross section. These flaws may lead to lower strength in the printed bars than those fabricated at 40°C. On the other hand, bars fabricated at 40°C have smaller flaws than those fabricated at -20°C or even have no flaws such as samples #1 and # 2 in Table 8. But a few of big flaws may occur when fabricating is done at 40°C, such as sample #5 shown in Table 8, Table 9 and Fig. 7b, which leads to a larger standard deviation in the mechanical properties.

Table 7. Mechanical properties and relative density of standard A bars fabricated at -20°C

#	Flexural Strength (MPa)	Flexural Modulus (GPa)	Relative Density (%)
1	334	261	90.48
2	325	259	93.32
3	303	356	91.34
4	269	285	91.41
5	268	240	91.18
Average	300	280	91.55
Standard Deviation	28	40	0.95

Table 8. Mechanical properties and relative density of standard A bars fabricated at 40°C

#	Flexural Strength (MPa)	Flexural Modulus (GPa)	Relative Density (%)
1	406	273	97.18
2	361	316	97.11
3	348	308	96.15
4	346	353	97.31
5	232	306	95.92
Average	338	311	96.73
Standard Deviation	57	25	0.58

Table 9. Calculated and measured maximum flaw size for the standard A bar

Standard A Bar	Calculated Maximum Flaw Size (μm)	Measured Maximum Flaw Size (μm)
Bars Fabricated at 40°C	Bar #3: 84	Bar #3: 54
	Bar #4: 85	Bar #4: 84
	Bar #5: 189	Bar #5:177
Bars Fabricated at -20°C	Bar #2: 96	Bar #2: 66
	Bar #3: 110	Bar #3: 91
	Bar #4: 141	Bar #4: 116

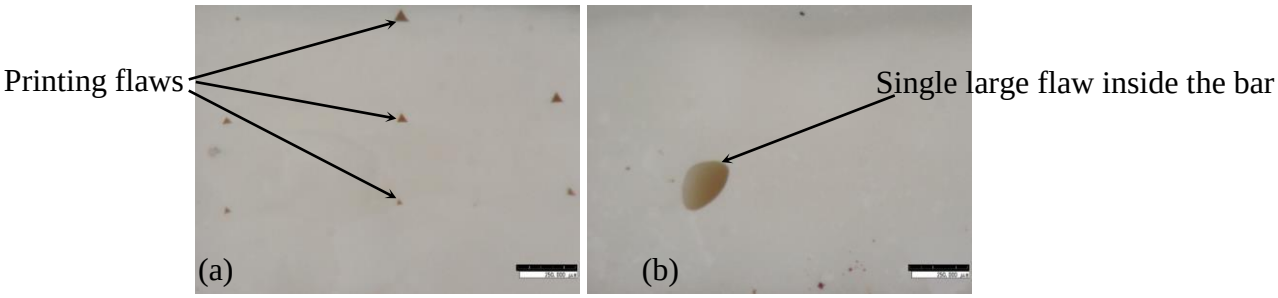

Figure 7. Cross-section of (a) bar fabricated at -20°C and (b) bar fabricated at 40°C

The theoretical modulus could be calculated using Nielsen's relationship of elasticity for porous ceramic materials as follows:

$$E = E_0 \frac{(1-P)^2}{1+\left(\frac{1}{\rho}-1\right)P} \quad (2)$$

where E_0 is the pore-free elastic modulus, P is the porosity in volume percent and ρ is Nielsen's shape factor (0.4). Based on the standard A bar measured results in Tables 7 and 8 and assuming a modulus of 380 GPa [20] for fully dense (100% density) Al_2O_3, the bars fabricated at 40°C had 3.27% on average, and the bars fabricated at -20°C had 8.45% porosity. By using Eq. (2), the theoretical modulus calculated for bars fabricated at 40°C was 339 GPa, and for the bars fabricated

at -20°C was 282 GPa. The experimentally measured flexural moduli in Tables 7 and 8 agreed fairly well with the theoretically calculated values.

Microstructure and Ice Crystal Formation

The SEM image of bars fabricated at -20°C revealed that several cracks spanned the entire bar (Fig. 8a). These cracks occurred because ice crystals formed at the boundary of each filament during freezing. Then the boundaries of neighboring filaments were not bonded strongly. Fig. 8b shows an image of the side of a bar fabricated at -20°C, and this image indicates ice crystal voids.

Bars fabricated at -20°C without using a nozzle had a warmer temperature (~ -15°C) inside the filament before they were fully frozen. The warmer temperature led to more formation of ice crystal voids [21, 22]. Figure 9 shows that the voids were larger and there were more voids than bars fabricated at -20°C with using a nozzle.

The SEM of bars fabricated at 40°C shown in Fig. 10 showed that there might be air bubbles present inside the bar, and the overall microstructure was similar to that of pressed pellets.

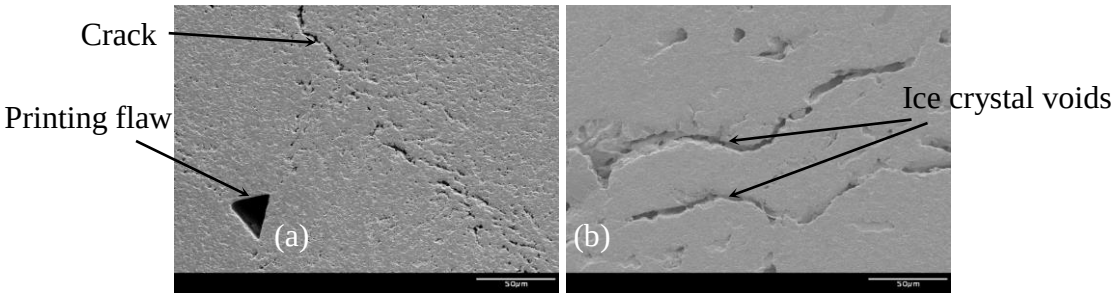

Figure 8. Bars fabricated at -20°C (at 350x zoom): (a) cross-section view and (b) side view

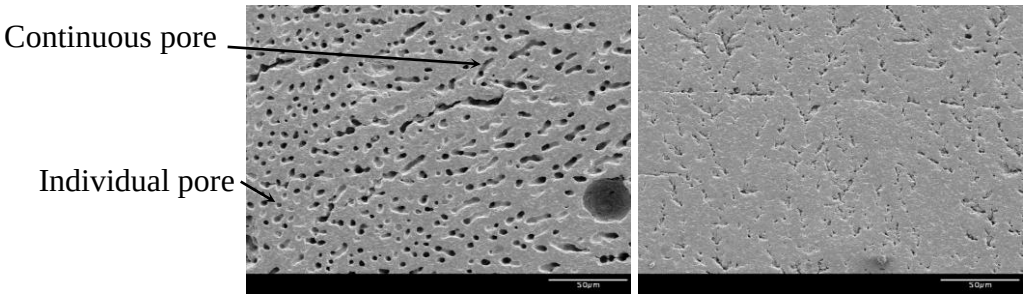

Figure 9. Bars fabricated at -20°C without using a nozzle (at 350x zoom): (a) side view and (b) cross-section view

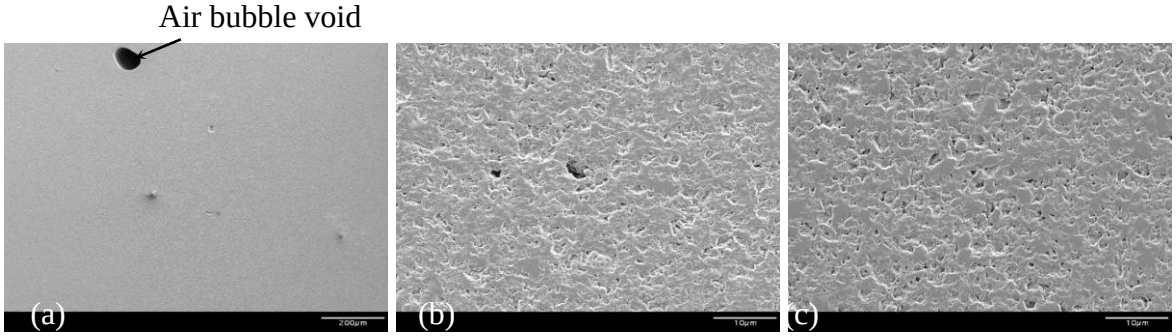

Figure10. Cross-section of bars fabricated at 40°C (a) 100x zoom and (b) at 3000x zoom ;(c) cross-section of pressed pellet 3000x zoom

Conclusion

This paper discusses the effects of temperature on ceramic parts produced by freeform extrusion fabrication. The parts fabricated at 40°C achieved relative density, flexural modulus, and flexure strength of 96.73%, 311 GPa, and 338 MPa, respectively. The parts fabricated at -20°C attained the relative density, flexural modulus and flexure strength of 91.55%, 280 GPa and 300 MPa, respectively. At 40°C, the minimum deposition angle achieved was 50^{o} at 38 mm bottom diameter, and at -20°C the minimum deposition angle achieved was 28^{o} at the same bottom diameter. The test bars fabricated at 40^{o}C and at -20^{o}C both have high flexural strength, Young's modulus, and relative density. The test bars fabricated at 40^{o}C have slightly higher mechanical properties. The hollow cones fabricated at -20^{o}C have smaller minimum deposition angles than those fabricated at 40^{o}C, indicating the greater capability of a freezing environment for fabricating larger and more complex parts without use of support (sacrificial) material. The analysis of the SEM images of the fabricated parts helps understand the formation of ice crystals when fabricating parts by the freeform extrusion fabrication process at freezing temperatures.

References

[1] Jacobs, P. F., *Rapid prototyping and manufacturing: fundamentals of stereolithography*, 1st Ed., Society of Manufacturing Engineers (1992).

[2] Guo, N., and Leu, M. C., "Additive manufacturing: technology, applications and research needs," *Frontiers of Mechanical Engineering*, Vol. 8, No. 3, Pp. 215-243 (2013).

[3] Noguera, R., Lejeune, M., and Chartier, T., "3D fine scale ceramic components formed by ink-jet prototyping process," *Journal of the European Ceramic Society*, Vol. 25, No.12, Pp. 2055-2059 (2005).

[4] Griffith, M. L., and Halloran, J. W., "Freeform fabrication of ceramics via stereolithography," *Journal of the American Ceramic Society*, Vol. 79, No. 10, Pp. 2601-2608 (1996).

[5] Grau, J., Moon, J., Uhland, S., Cima, M. J., and Sachs, E., "High green density ceramic components fabricated by the slurry-based 3DP process," In *Solid Freeform Fabrication Symposium*, Pp. 371-378 (1997).

[6] Lewis, J. A., Smay, J. E., Stuecker, J., and Cesarano, J., "Direct Ink Writing of Three-Dimensional Ceramic Structures," *Journal of the American Ceramic Society*, Vol. 89, No. 12, Pp. 3599-3609 (2006).

[7] Griffin, E. A., and McMillin, S., "Selective laser sintering and fused deposition modeling processes for functional ceramic parts," In *Proceedings of the Solid Freeform Fabrication Symposium*, Vol. 6, Pp. 25-30 (1995).

[8] Cesarano, J., "A review of robocasting technology," In *MRS Proceedings*, Cambridge University Press, Vol. 542, Pp. 133. (1998).

[9] Agarwala, M. K., Jamalabad, V. R., Langrana, N. A., Safari, A., Whalen, P. J., and Danforth, S. C., "Structural quality of parts processed by fused deposition," *Rapid Prototyping Journal*, Vol. 2, No. 4, Pp. 4-19 (1996).

[10] Lous, G. M., Cornejo, I. A., McNulty, T. F., Safari, A., and Danforth, S. C., "Fabrication of piezoelectric ceramic/polymer composite transducers using fused deposition of ceramics," *Journal of the American Ceramic Society*, Vol. 83, No. 1, Pp. 124-28 (2000).
[11] Denham, H. B., Cesarano III, J., King, B. H., and Calvert, P., August, "Mechanical behavior of robocast alumina," In *Proceedings of the Solid Freeform Fabrication Symposium,* Pp. 589-596 (1998).
[12] Huang, T., Mason, M. S., Zhao, X., Hilmas, G. E., and Leu, M. C., "Aqueous-based freeze-form extrusion fabrication of alumina components," *Rapid Prototyping Journal*, Vol. 15, No. 2, Pp. 88-95 (2009).
[13] Huang, T., Mason, M. S., Hilmas, G. E., and Leu, M. C., "Freeze-form extrusion fabrication of ceramic parts," *Virtual and Physical Prototyping*, Vol. 1, No. 2, Pp. 93-100 (2006).
[14] Rahaman, N., *Ceramic processing*. 1st Ed., John Wiley & Sons, Inc., (2006).
[15] Singh, B. P., Bhattacharjee, S., Besra, L., and Sengupta, D. K., "Evaluation of dispersibility of aqueous alumina suspension in presence of Darvan C," *Ceramics international*, Vol. 30, No. 6, Pp. 939-946 (2004).
[16] Saravanan, L., and Subramanian, S., "Surface chemical studies on the competitive adsorption of poly (ethylene glycol) and ammonium poly (methacrylate) onto alumina," *Journal of colloid and interface science*, Vol. 284, No. 2, Pp. 363-377 (2005).
[17] Sofie, S. W., and Dogan, F., "Freeze casting of aqueous alumina slurries with glycerol," *Journal of the American Ceramic Society*, Vol. 84, No. 7, Pp. 1459-1464 (2001).
[18] Zhao, X. Y., Mason, M. S., Huang, T. S., Leu, M. C., Landers, R. G., Hilmas, G. E., Easley, S. J, and Hayes, M. W., "Experimental Investigation of Effect of Environment Temperature on Freeze-Form Extrusion Fabrication," In *18th Annual Solid Freeform Fabrication Symposium*, Pp. 6-8 (2007).
[19] Wachtman, J. B., Cannon, W. R., and Matthewson, M. J., *Mechanical properties of ceramics*, 2nd Ed., John Wiley and Sons (2009).
[20] Richerson, D., *Modern ceramic engineering: properties, processing, and use in design*, 3rd Ed., CRC press (2005).
[21] Deville, S., "Freeze-Casting of Porous Ceramics: A Review of Current Achievements and Issues," *Advanced Engineering Materials*, Vol. 10, No. 3, Pp. 155-169 (2008).
[22] Deville, S., Saiz, E., and Tomsia, A. P., "Ice-templated porous alumina structures" *Acta Materialia*, Vol. 55, No. 6, Pp. 1965-1974 (2007).